Design and Development of a Positioning Robot for use as a Surgical Debridement Method

by

Diana M Rosales

Submitted to the Department of Mechanical Engineering in Partial Fulfillment of the Requirements for the Degree of

Bachelor of Science in Mechanical Engineering

at the

Massachusetts Institute of Technology

June 2015

Signature redacted

Signature of Author: _____

Department of Mechanical Engineering
May 22, 2015

Signature redacted

Certified by: _____

Ian W. Hunter
Hatsopoulos Professor of Mechanical Engineering
Thesis Supervisor

Signature redacted

Accepted by: _____

Anette Hosoi
Professor of Mechanical Engineering
Undergraduate Officer

Design and Development of a Positioning Robot for use as a Surgical Debridement Method

by

Diana M Rosales

Submitted to the Department of Mechanical Engineering
on May 22, 2015 in Partial Fulfillment of the
Requirements for the Degree of

Bachelor of Science in Mechanical Engineering

Abstract

Debridement, the act of removing dead tissue and debris from wounds, is critical to ensure the wound healing process is resumed in chronic wounds and wounds that are stuck in the healing process. This thesis investigates the positional accuracy of a positioning robot for future development as a hydro-surgical debridement robot that runs autonomously. After completion and assembly of the mechanical structure of the robot, two different infrared sensors, the VCNL4000 Infrared Proximity sensor and the Sharp GP2Y0A41SK0F Short Range Proximity Sensor were used and tested for their distance measuring capabilities. Both sensors were found unsuitable to accurately measure and detect a distance of 1mm from the surface measured and are not recommended for future iterations of the robot. Different sensor recommendations are made to continue the development and exploration of this robot for use as a debridement method.

Thesis Supervisor: Ian W. Hunter
Title: Hatsopoulos Professor of Mechanical Engineering

Acknowledgements

First, I would like to thank Professor Ian Hunter for giving me the opportunity work and learn with him in his lab. I would also like to thank my thesis supervisor Ashley Brown for the guidance and support she provided me with for this project. I would also like to extend a big thank you to all the members of the Bioinstrumentation lab for the help, advice, and time they shared with me. A big thank you to Ashin Modak for the help he provided throughout the development of this thesis.

Contents

List of Figures

Chapter 1

Introduction

Debridement is the act of removing dead tissue and debris from wounds. It is critical for wounds that are stuck in the healing process to undergo debridement to restart and accelerate the healing process [1]. Chronic wounds, such as pressure ulcers and diabetic foot ulcers, require debridement more often than other type of wounds [2]. Debridement is critical procedure for chronic wounds that reduces the probability of amputation for a patient [3]. Ulcers are the most common type of chronic wound, with an "...estimated 2.5 million Americans affected by venous ulcers, 1.3 to 3 million suffer from pressure ulcers, and 1 million diabetics are at risk for developing neuropathic ulcers over any 3 year period" [4]. Although there are various methods of debridement, the wound itself and the skill level of a practitioner will determine the method of debridement used on a wound [2].

Making debridement robotically operated would remove the dependency of a practitioner's experience on the method of debridement used. A robotic debridement process would also reduce the risk of surgeon fatigue caused by debridement being a tedious task [5]. A study done by a team at the University of California, Berkeley

determined that surgical debridement is a suitable task for autonomous operation [5].

This thesis presents explores the use of a positioning robot for future application as a hydro-surgical debridement robot. Chapter 2 explains the wound healing process, current debridement techniques, and the increasing presence and use of robots in medical settings. Chapter 3 highlights design requirements for a debridement robot to create the design requirements for the required positioning robot. Chapter 4 goes into further detail of the mechanical and electrical design of the robot and Chapter 5 presents the testing and performance of the robot. Chapter 6 concludes with a discussion of a review of the robot and recommendations for future development.

Chapter 2

Background

2.1 Wound Healing

Skin is made up of two layers of tissue. As shown in Figure 2.1, the topmost layer is the epidermis, followed by the dermis. An acute wound occurs when there is a breach in the epidermis [1]. To heal the wound, the body undergoes four stages of wound healing. The first stage of healing, the coagulation phase, is initiated by platelets that migrate to the site of the wound to stop the bleeding and to release multiple growth factors. Inflammatory cells are attracted to the wound during and the inflammatory phase begins. During this phase, neutrophils and macrophages destroy bacteria and the damaged extracellular matrix is degraded. During the cell proliferation stage, a provisional wound matrix is made. The matrix does not become integrated until all of the damaged proteins are removed. Finally, the remodeling stage continues to synthesize the new extracellular matrix and the appearance of a scar is improved. The entire process can take multiple months [1].

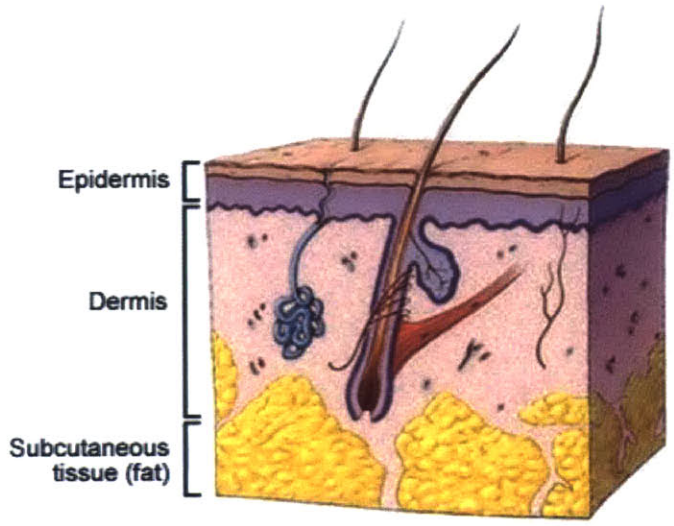

Figure 2.1: Image depicting the layers of the skin and underlying connective tissue. Photo reproduced from [6].

2.2 Chronic Wounds and Debridement

Some wounds do not complete the healing process because of their inability to move from one healing stage to the next. Chronic wounds, for example, are thought the be stuck at the inflammatory stage and cannot effectively remodel the extracellular matrix [1].

Wound bed preparation is essential to treat chronic wounds. It clears the wound, making it resemble an acute wound, so it can restart the healing process [1]. This is done by the process of debridement, which clears the dry and hard necrotic tissue from the wound and removes any biofilms that prevent the wound from healing [3].

Debridement is also important because the removal of the dead tissue allows for more accurate wound assessments and infections are easier to detect. It can also accelerate the wound healing process in a natural way [2].

2.3 Current Debridement Techniques

There are various types of debridement methods physicians use for different wound types.

Sharp debridement removes necrotic tissue with the use of scalpels and other metal instruments. It is done by a well-trained clinician and is used for quick removal of tissue [4]. This method is favored for large wounds, but can be painful for the patient and can damage tendons and nerves [1]. A downside to this method is that healthy tissue is sometimes removed due to the invasive nature of the practice [3].

Autolytic debridement happens naturally within the body. The body's natural enzymes are attracted to the wound site and break down damaged tissue [1].

Enzymatic debridement uses enzymes to break down the degraded or weak extracellular matrix. It is the most useful technique for large wounds where surgery cannot be used [1].

Mechanical debridement removes both healthy and devitalized tissue with wet-to-dry dressings. The dressing is applied to a wound and the top most layer of tissue is removed when the dressing is peeled off. This method can also be painful to patients.

Biological debridement removes necrotic tissue by applying larvae to the wound. The maggots eat away at the damaged tissue they broke down [1].

The advantages and disadvantages for these techniques are summarized in Table 2.1. The important factors needed to help determine which debridement method is the best to use are size and amount of tissue to remove, the location of the wound, and the skill level of the practitioner [2].

Table 2.1: Comparison of different debridement techniques where 1 = Most Appropriate and 4 = Least Appropriate. Taken from [7].

	Autolytic	Surgical	Enzymatic	Mechanical
Speed	4	1	2	3
Tissue Selectivity	3	2	1	4
Painful Wound	1	4	2	3
Exudate	3	1	4	2
Infection	4	1	3	2
Cost	1	4	2	3

Another debridement technique not included in the table above is hydro-surgery, or the use of a jet streams to remove tissue. This method is most praised for its ability to selectively remove necrotic tissue [4] and because it is well-suited for smaller areas such as on the hands and feet [2]. The fact that this method can selectively target dead tissue makes it a very desirable debridement method, especially given that two of the biggest challenges with all debridement techniques is the lack of tissue selectively and blood loss from the procedure [4].

2.4 Dual Nozzle Debridement Instrument

The Bioinstrumentation lab is currently developing a dual nozzle instrument to perform hydro-surgery debridement. The device, shown in Figure 2.1, uses two high pressured water jets to excise tissue. The two jet streams from the nozzles intersect and make a V cut out of the tissue, as shown in Figure 2.2. The device can be configured to change the width and depth of the cut depending on the distance between the two nozzles and the angle of the jet streams.

The average depth of cuts made with the device ranged from 1.2 mm to 1.3 mm when cut at a velocity of 4 mm/s [8]. The depth of the cut tissue can also depend

on the type of tissue being cut, whether it is soft tissue or hard and dry tissue [8].

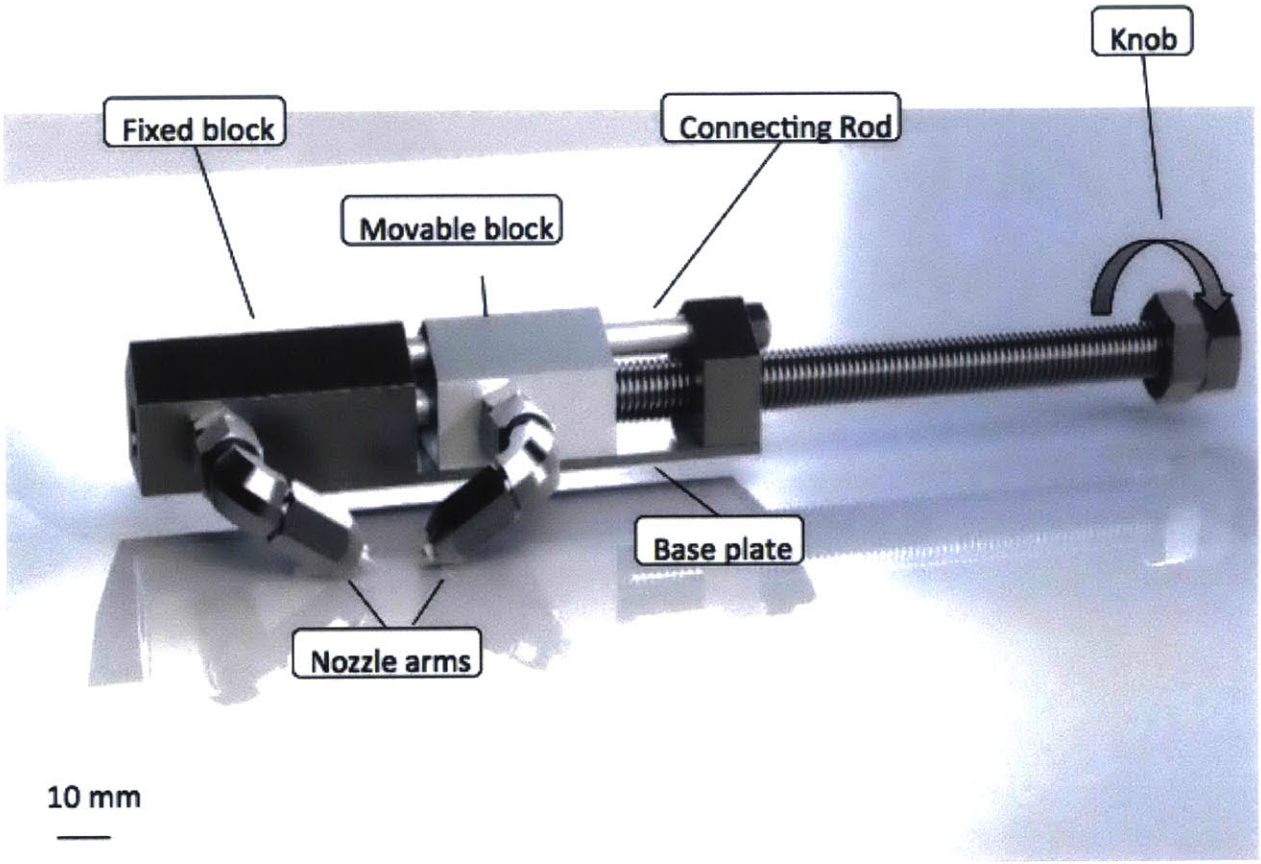

Figure 2.2: Image rendering of the dual nozzle debridement instrument. Image taken from [8].

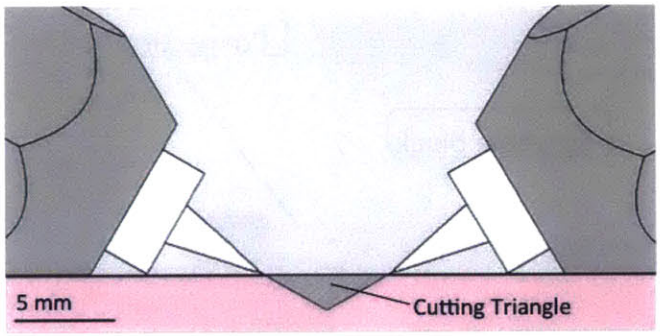

A

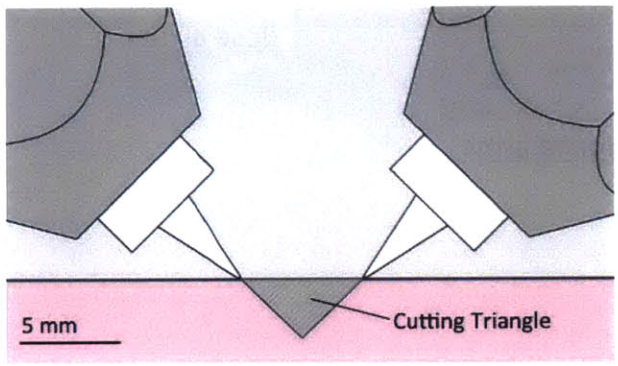

B

Figure 2.3: The two nozzles of the device are placed on the tissue to be cut. The high pressured jet streams intersect each other in the tissue and cut the tissue in a triangular shape as shown in the images. Figure A and B show two different configurations of the nozzle orientation and position that allow for two different cut shapes. Photo reproduced from [8].

Chapter 3

Development of Surgical Debridement Robot

3.1 Problem Statement

Although there is much research on various debridement techniques, there is still room for improvement. The ideal debridement method is easy to use, precise, quick, safe, and can differentiate and target necrotic tissue [4].

This study will explore the use of a robot for hydro-surgical debridement. The robot will be designed for use with the dual nozzle debridement instrument currently under development at the MIT Bioinstrumentation lab. Aside from correctly detecting and removing necrotic tissue from a wound, the robot must also position itself against a wound on a surface of the body. It is important the robot's end effector stay parallel to the contour on the body it is removing tissue from to remove the correct amount of tissue from the wound. Because the body does not have flat surfaces, it is important the robot position and orient itself well to the surface of a wound.

This thesis will therefore focus on the position and orientation of the end effector relative to a surface. Aside from further development of the degrees of freedom and positional accuracy of the robot, future work for the robot will include the ability to distinguish between healthy and unhealthy tissue to remove from a wound.

3.2 Design Requirements

The design requirements for a robotic hydro-surgical debridement device were derived from the problem statement and are summarized in Table 3.1.

Table 3.1: Detailed design requirements for a robotic hydro-surgical debridement device.

Name	**Description**
Removes necrotic tissue	Device can distinguish between unhealthy and healthy in a wound. This can be done on a wound on any part of the body.
Minimize Infection to Wound	Procedure should decrease risk of infection to wound.
Minimizes Pain	Device should not be any more painful than sharp debridement technique and should aim to be as painless as possible.
Quick Procedure	The device should allow for a debridement procedure that is as quick as sharp debridement technique.
Simple to Use	User friendly and simple for a physician, surgeon, or nurse to use.
Reusable	If designed to be reusable, parts should be compatible with sterilization techniques.
Biocompatible	If any part comes in contact with skin, it should follow FDA guidelines for biocompatibility.
Safe Failure Mode	Device will not cause harm to a patient should it fail for any reason.
Reliability	Device should perform functions repeatedly.
Cost Effective	The device should be cost-effective for hospitals, manufacturer, and patients.

However, as mentioned before, this study will only focus on the development of a surface detecting and following robot. This specific design objective resulted in the design requirements for the robot and are outlined in Table 3.2.

Table 3.2: Design requirements for a positioning robot meant for use as a debridement robot.

Names	Description
End Effector maintains distance, D, away from surface	End-effector of robot must maintain a user specified distance, D, away from the surface of the skin at all times.
Autonomous end effector positioning	End-effector should position itself in correct orientation (parallel) relative so the surface it is following.
Reliability	Robot should perform its function in a consistent and repeatable manner.
Maximize work Space	End-effector work space should be maximized to allow for use on various surfaces of the body.
Fluid, continuous motion	Robot should move in a continuous manner to properly follow a surface without breaks in motion.
Quick positioning	Robot should move quickly to minimize procedure time.
Safe Failure Mode	If robot comes into contact with a surface, it will stop.
Simple User Interface	Robot should be easy to use.
Similar aspect to final product	Robot concept should have some function or design aspect that most resembles a design parameter needed in a final debridement robot.

The two major design challenges for this project is the mechanical structure that allows for the required movements described above and the sensors that will detect distance accurately.

3.3 Concept Generation

Six design concepts for the mechanical structure of the device were generated based on the functional requirements outlined in Section 3.2. A concept will be selected for use in this study in Section 3.4 with the a Pugh chart [10]. The biggest consideration during brainstorming was to maximize the work-space of the end-effector.

3.3.1 Overhead Arm- Fixed End

The first concept generated is a two linkage arm attached to a linearly translating piece. The translating piece is held at a height above the floor with the two linkage arm hanging from it. The end-effector is fixed at the end of the two-linkage arm. The concept is shown in Figure 3.1. The numbers in the image and on all subsequent concept images is a count of the number of actuators each design needs.

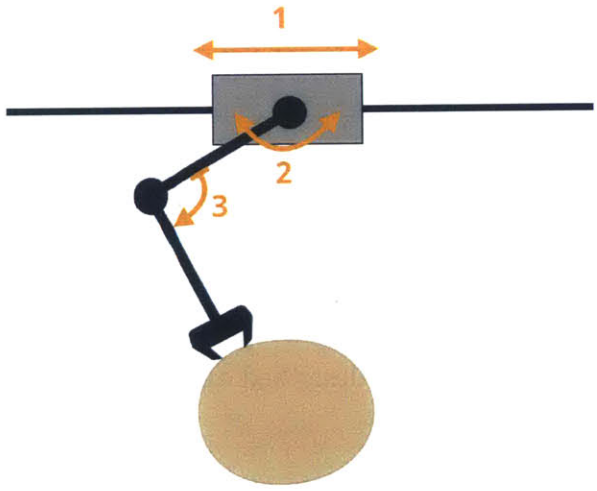

Figure 3.1: Translating overhead arm with a fixed end-effector. The concept has three degrees of freedom.

The top-most arm for this concept is imagined to be capable of complete rotations to maximize the work-space of the end-effector. If this were not the case, the robot could have difficulty reaching the right side of the forearm if it translates from left to right.

3.3.2 Overhead Arm- Rotating End

The second concept is similar to the first one, except the end-effector has a rotational degree of freedom. This concept is shown in Figure 3.2.

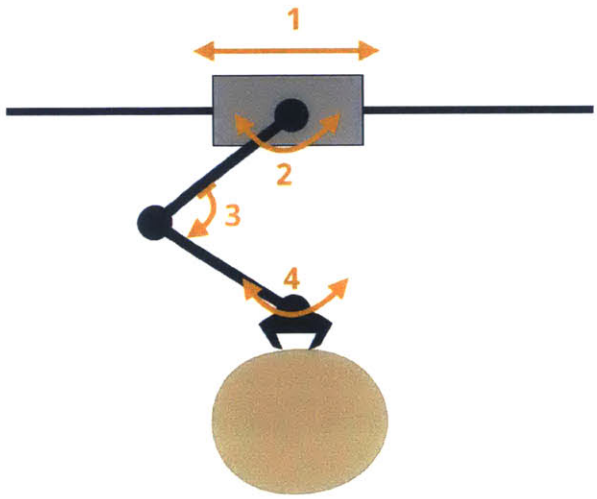

Figure 3.2: Translating overhead arm with a rotating end-effector.

The risks considered for the first concept apply to this one as well. This concept requires one more actuator than the first one and would therefore have slightly more complicated kinematics and controls needed.

3.3.3 Linear Motion Robot

The third concept generated is composed linear components with a rotating end-effector. The linear motion robot concept, like the previous two concepts, has a moving piece that moves along a linear guide horizontally. A linearly actuated piece is mounted vertically to the horizontal moving part and has a rotating end-effector on

its end. The concept is shown in Figure 3.3. The linear components of this concept allow for simpler kinematics compared to the previous concepts.

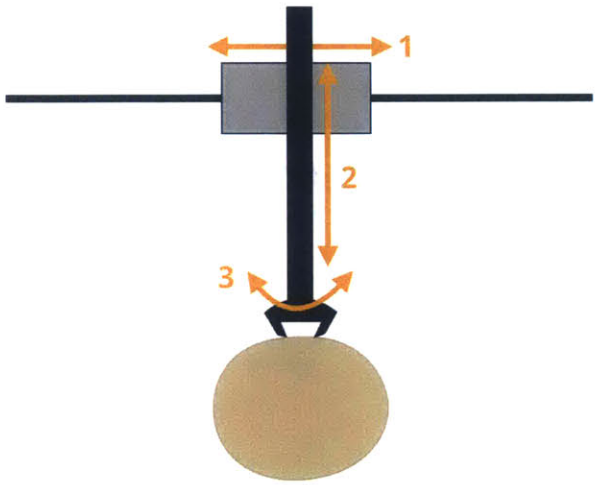

Figure 3.3: Linear vertical and horizontal actuation with a rotating end-effector. Vertical piece is mounted onto the linear horizontal piece.

3.3.4 Fixed Rotating Arm

The fourth concept generated is a two-linkage arm fixed to the ground with a rotating end-effector. The concept, which only has rotational elements, is shown in figure 3.4. The rotating end-effector allows the robot to increase the available work-space compared to a same design without a rotating end. However, a big concern for this concept is its limited access to the right side of the forearm.

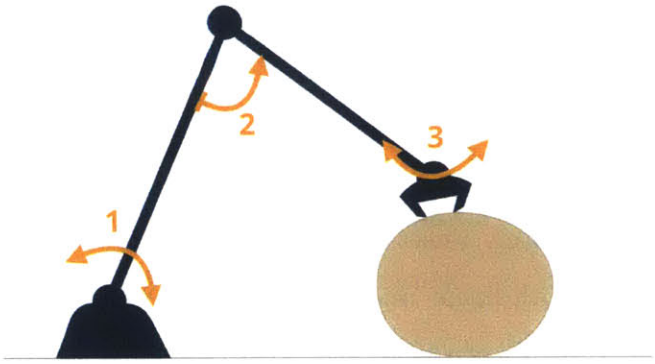

Figure 3.4: Fixed 2-linkage rotating arm with rotating end-effector.

3.3.5 Prismatic and Revolute Joint Arm

To address the limited access of the fixed arm to the right side in concept four, the concept was redesigned such that it has prismatic joints as well as revolute ones. In this way, the arm could extend itself as necessary to reach the other side of the forearm. Figure 3.5 depicts the concept idea as described.

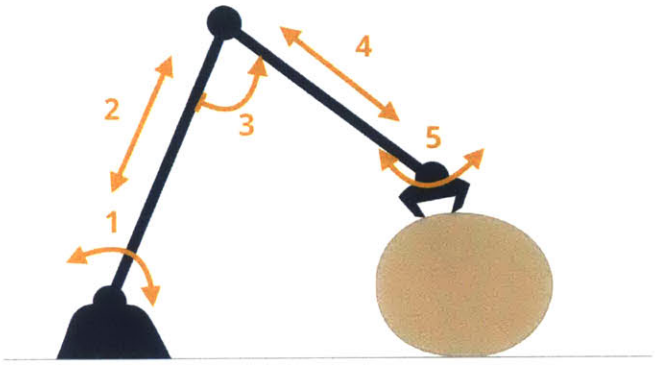

Figure 3.5: Fixed arm with prismatic and revolute joints and a fixed end-effector.

This concept immediately raises concerns over its kinematics and manufacturing. The concept has both linear and rotating movements that add complexity to the kinematics and controls of the robotic arm. Similarly, the manufacturing and assembly of such a device would involve a large number of components.

3.3.6 Two Coupled Arms

The last concept generated has two coupled arms that are fixed on either side of the forearm. The end-effector is attached to the end of both arms. Figure 3.6 shows the concept as first realized.

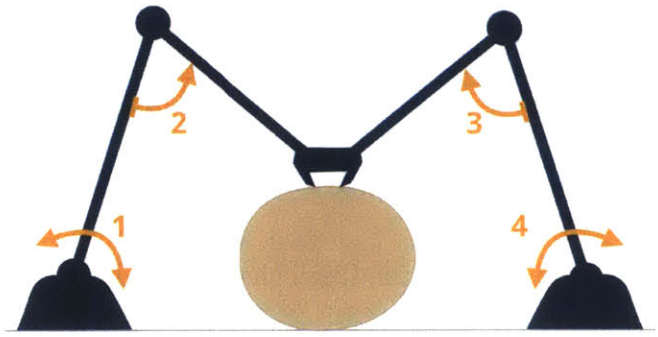

Figure 3.6: Two fixed and coupled arms with a fixed end-effector.

The kinematics and coupling of the arms are crucial for this design. The design was inspired by the Delta desktop 3D printer shown in Figure 3.7. The difference between the concept and the printer is that the nozzle of the printer is meant to always face down. The printer's actuators are thus designed and controlled to make sure the nozzle is always parallel to the floor. The robot designed for this study must have the ability to face different orientations and it is unclear whether the robot can do that with the concept presented or if it would need additional actuators to allow for additional degrees of freedom.

3.4 Concept Selection

After all 6 methods were generated, the Pugh concept selection method was used to select one of the concepts. With this selection method, all concepts are compared to a datum against the same set of evaluation criteria based on the functional requirements. It is important the criteria in the Pugh chart is not redundant so the concept ranking is as accurate as possible.

The evaluation criteria used for the Pugh chart was taken directly from the functional requirements summarized in Table 3.2. Functional requirements related to sensor selection and actuation, such as "accurately measure distance," were omitted from the table since they do not pertain to the mechanical design of the structure. Additionally, the following three evaluation criteria parameters were added to the Pugh chart: easy to manufacture, simple kinematics, and cost.

Concept 1, the overhead arm with a fixed end-effector, was chosen as the datum for the selection matrix because of the author's previous understanding of a similar design.

Concept 1, the overhead arm with a fixed end-effector, and Concept 3, the linear motion robot, tied with the highest score. Upon further inspection, it was observed that the tradeoff criteria for the two concepts are the concept's similarity to the final debridement robot and the simplicity of the kinematic design. Because the final design of the robotic debridement robot has not yet been conceived, a concept's similarity to the final design was difficult to evaluate. Due to this uncertainty, Concept 3, the linear motion robot, was chosen for its simple kinematics.

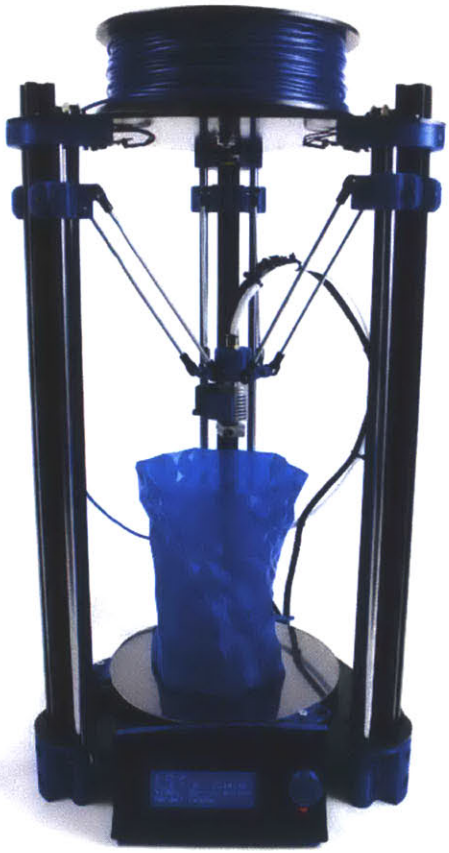

Figure 3.7: BCN3DR Desktop 3D printer with a three arm design. Photo taken from [9].

Chapter 4

Positioning of Robot

4.1 Robot Design

The robot was designed to have four degrees of freedom: X, Y, Z, and rotation of the end-effector. The Solidworks assembly of the complete design is shown in Figure 4.1 below [11].

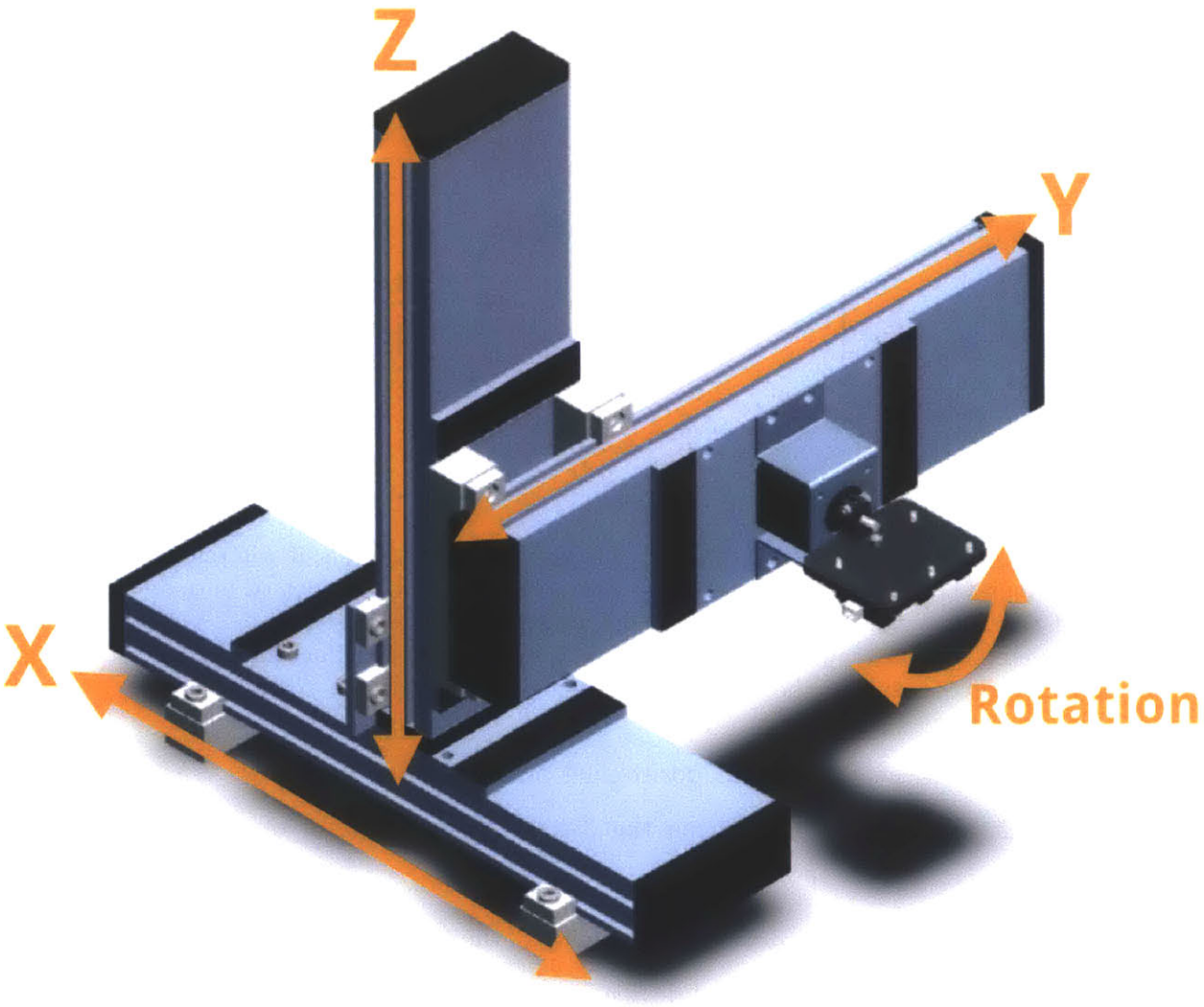

Figure 4.1: Complete Solidworks assembly of the robot design. The arrows depict the intended motion for each degree of freedom. The motors and their attachments are not included in the assembly.

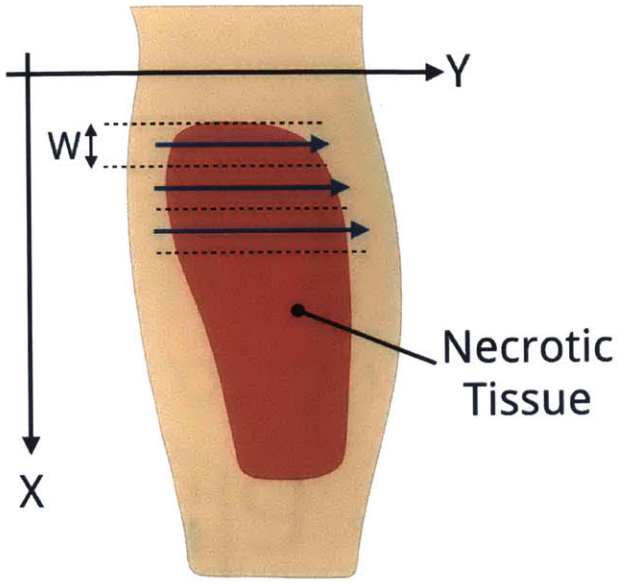

Figure 4.2: The robot moves such that at each position on the X-axis, it will remove tissue from a wound along the Y-axis in the direction of a blue arrow. The dotted lines on either side of the blue cutting paths represent the actual cuts made in the tissue. Once a cut is completed, the robot will move a distance W along the X-axis for the next cut. The distance W is the same as the width of the tissue removed from the wound.

The intended movement and positioning of the robot is as follows is shown in Figure 4.2. For a fixed position on the X-axis, the end-effector of the robot will move along the Y-axis at a constant speed of either 3 or 4 mm/s. The speeds were determined experimentally during development of the dual nozzle debridement device [8]. At 4 mm/s, the hydro-surgical device can excise tissue with an average depth of 1.2 to 1.3 mm [8]. The robot also has the ability to move along the Z-axis to account for changes in height of the surface it is cutting.

However, as mentioned in Section 3.1, the surface of the body is not flat. Figure 4.3 shows a schematic of a wound on the forearm and the trajectory the end-effector must take in the Y-Z plane to remove dead tissue from the wound. The trajectory

outlined in Figure 4.3 requires a rotational degree of freedom to be added to the to the design of the positioning robot. To explore how this could be achieved, a sensor plate was designed to be mounted on the linear carriage of the Y-axis linear stage, shown in Figure 4.4. The sensor plate is mounted onto the shaft of a stepper motor and holds three sensors in a linear array. The sensor mount is designed to hold three sensors to represent the three points in space that define a plane. The plane defined in space by the sensors, shown in Figure 4.5 could then be made parallel to the surface of a wound.

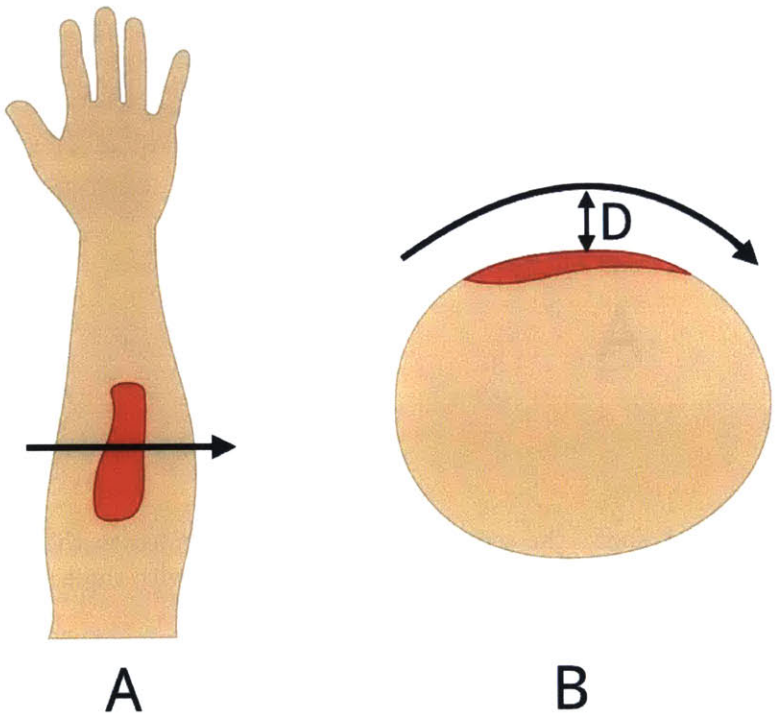

Figure 4.3: Left image shows the cutting path the robot will take to remove tissue from a wound on the forearm in the Y-axis. The actual trajectory the end-effector will take while moving along the Y-axis at a constant speed is shown on the right side on a cross-section of the forearm. Images are not to scale relative to each other.

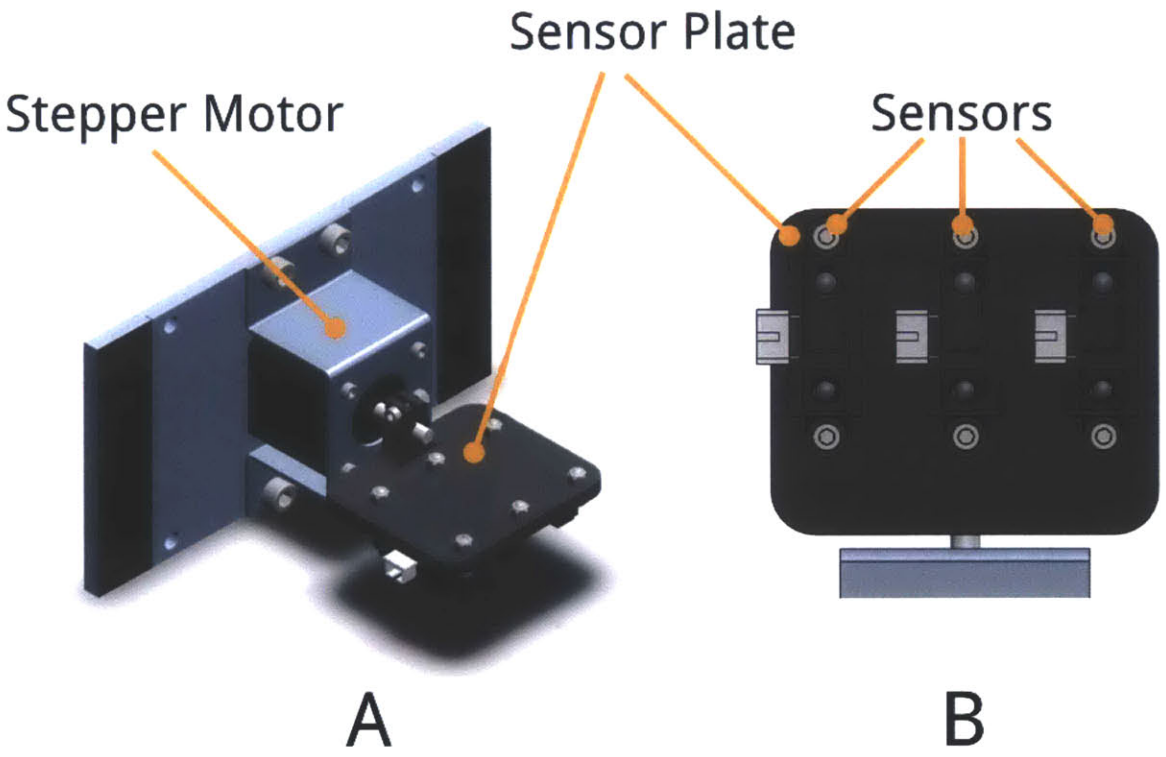

Figure 4.4: Figure A shows the sensor plate assembly mounted to the carriage of the Y linear stage. Figure B shows the bottom of the sensor plate with three sensors mounted in a linear array.

Figure 4.5 is an example of a simple contour on the body compared to one on the foot, for example. As mentioned in Chapter 1, ulcers, especially diabetic foot ulcers, are one of the most common types of chronic wounds [4]. Diabetic foot ulcers can be found on any surface of the foot, but are most commonly found on the bottom of the foot. Depending on the actual location of the ulcer on the foot, a three or four degree of freedom robot may not be able to position itself properly to remove devitalized tissue from the wound. For highly contoured surfaces such as the ones found on the foot, a robot with at least six degrees of freedom is needed.

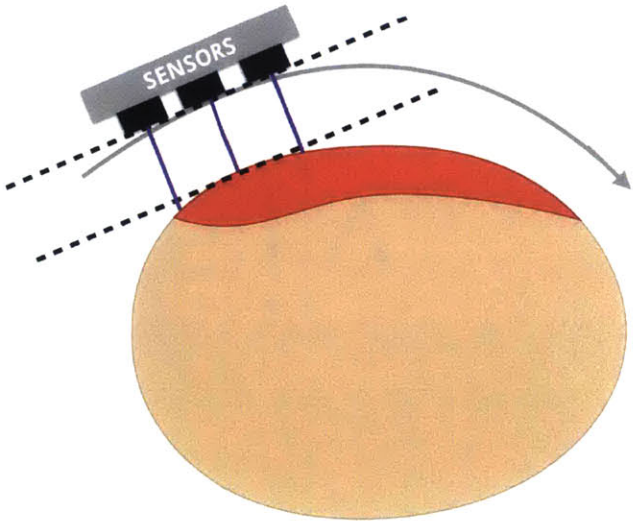

Figure 4.5: The figure shows how the sensors mounted on the sensor plate create a plane that can be moved to become parallel to the plane of the surface that needs to be cut.

This study will establish the positioning capabilities of the designed robot shown in Figure 4.1 with three degrees of freedom. Once the precision and repeatability of the robot's positioning are characterized, developments can be made in the future that explore the incorporation more degrees of freedom to the design, starting with

rotation.

The final assembled robot is shown in Figure 4.6. The linear motion for the X, Y, and Z axes is realized with linear ball-screw 404XR series stages from Parker Automation [12]. Each linear stage provides 150 mm of travel with 5 mm/revolution positioning from its ball-screw. The linear stage has a positional accuracy of 10 microns and a maximum screw speed of 60 revs/sec [12].

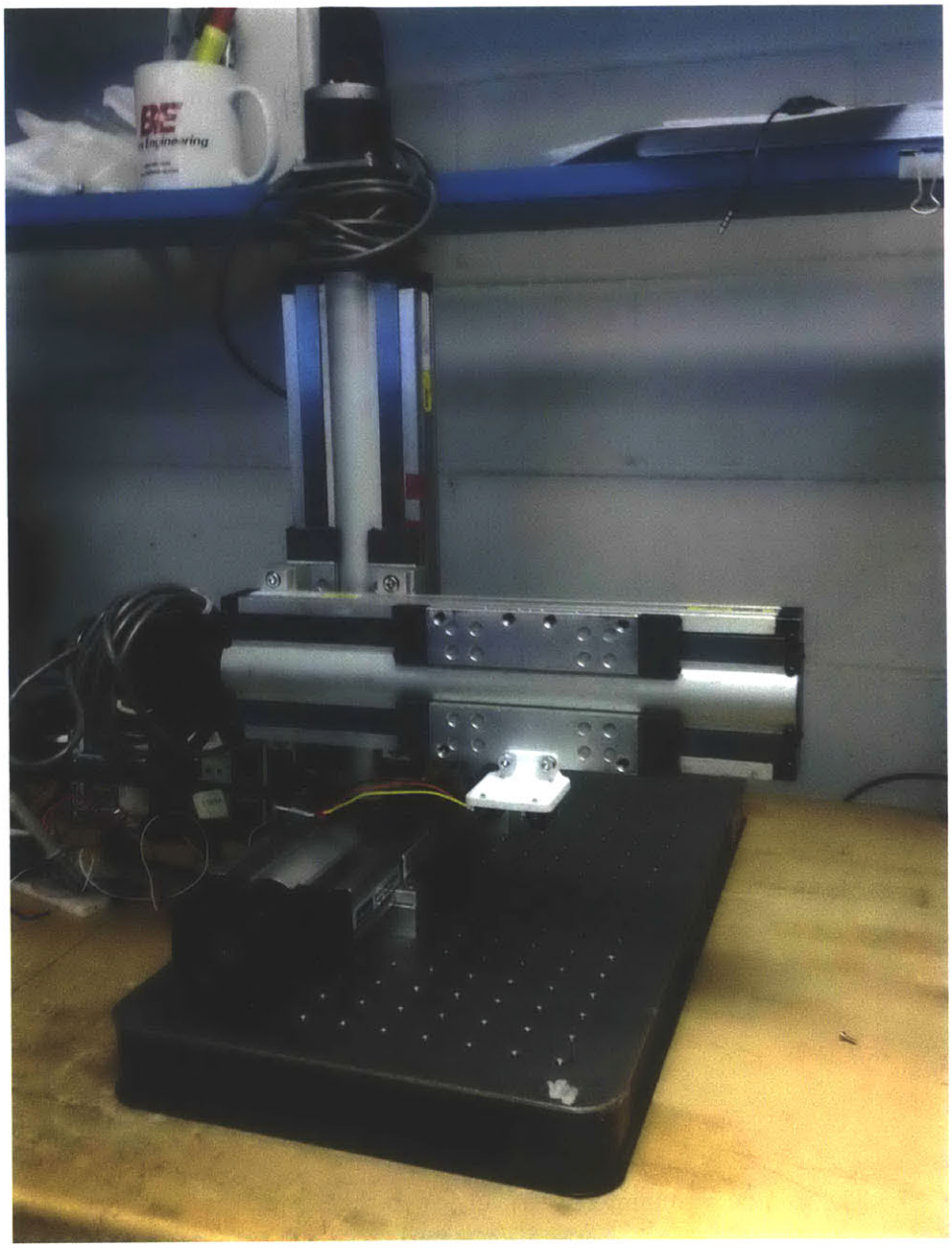

Figure 4.6: Image of the final assembled robot.

The linear stages are attached to each other via the accessory parts that allow for horizontal mounting. A corner bracket was machined to mount the Z-axis vertical to the X-axis as shown in Figure 4.7.

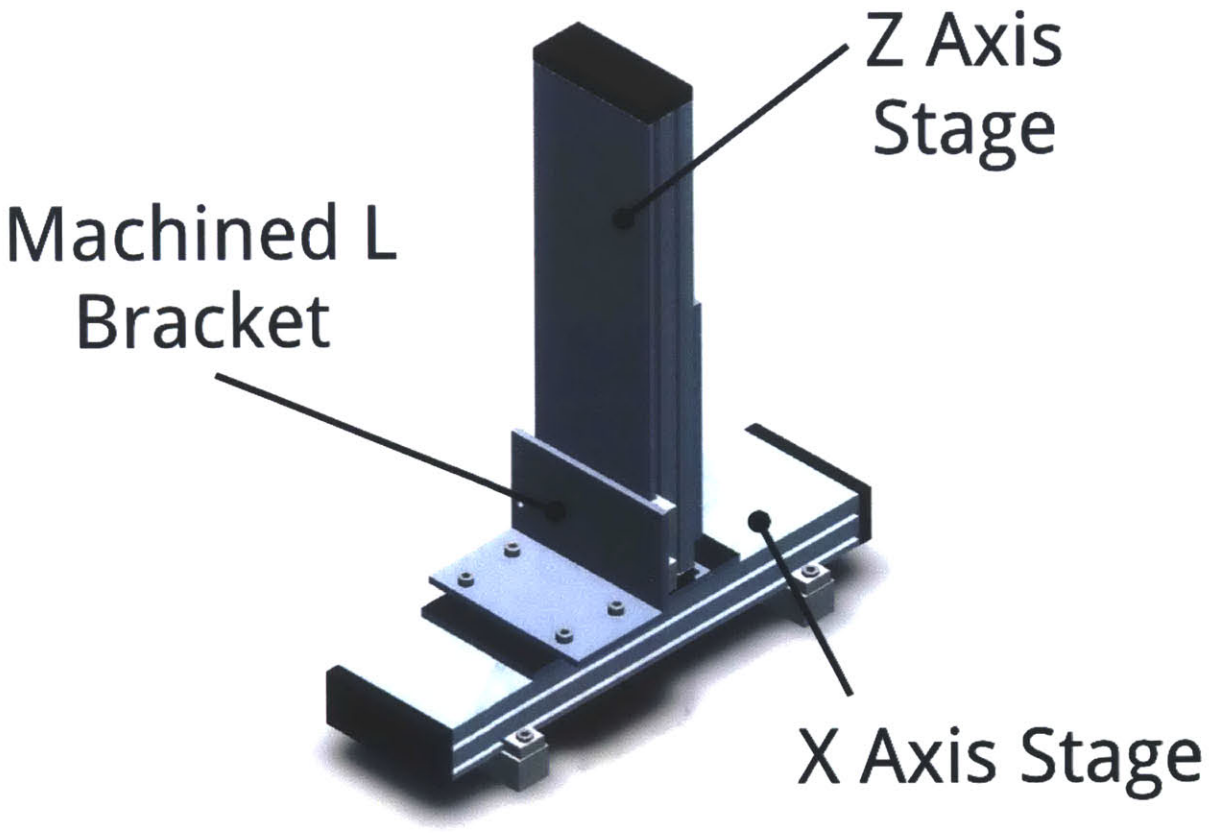

Figure 4.7: The Z-Axis is mounted vertically with respect to the X-axis with a corner bracket.

The end-effector of the robot has a total workspace of 424.3 mm in height, 435.5 mm in length along the X- axis, and 359 mm in width along the Y-axis, shown in Figure 4.8.

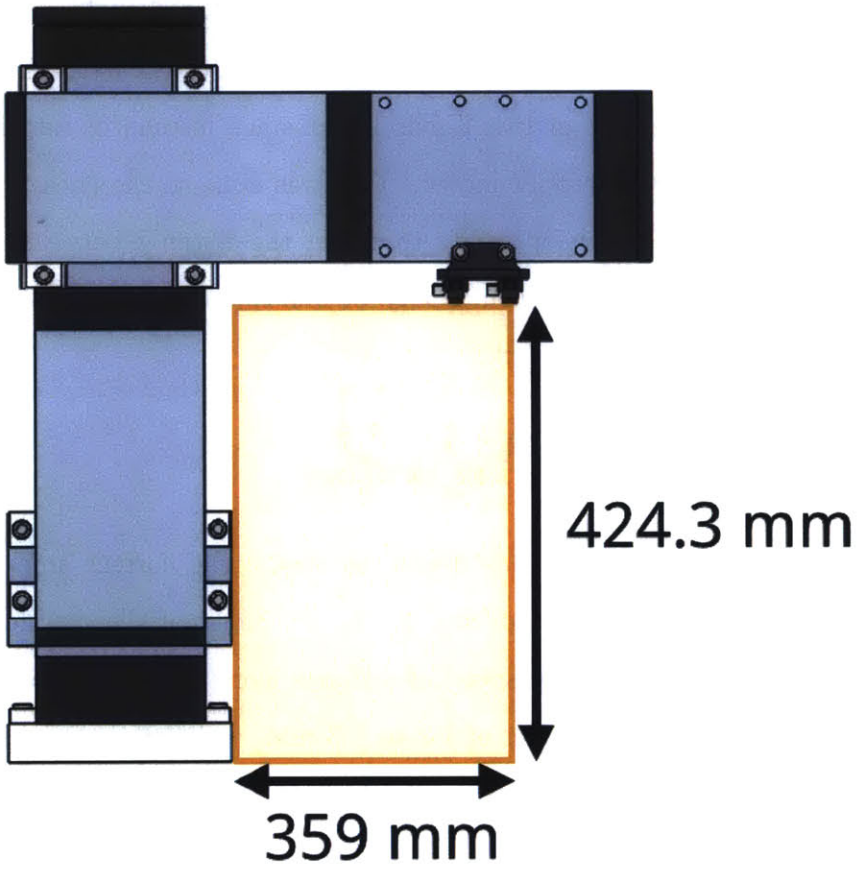

Figure 4.8: Available work space of the end-effector of the robot.

The linear stages are actuated by ZETA57-51 compumotors from Parker Automation[13]. The stepper motors are each driven by a ZETA4 micro-stepping driver from Parker-Motion that are used with a resolution of 10,000 steps/second [13]. All components were connected and controlled by an Arduino Uno [16].

Additionally, the sensor plate was modified for the assembly of the robot from the design presented in Figure 4.1. The sensor plate was redesigned to be rigidly attached to the carriage of the Y-axis linear stage instead of rotating around the shaft of an additional stepper motor. This was done so the chosen sensors for the robot could be evaluated for ability to detect the distance between a given surface and the sensor without the complexity of multiple degrees of freedom that could instead be tested in future work.

4.2 Distance Measuring Sensors

Positional accuracy of the end-effector to ensure the correct amount of tissue is removed from a wound. According to the developer of the double nozzle device, the nozzles require a cutting speed of 4 mm/s along the surface of the wound and have an average cutting depth of 1.2 to 1.3 mm . The study was then focused on the selection of a non-contact distance detecting sensor with a distance measuring resolution of at least 1mm.

The following sensors are the two most commonly used non-contact distance detecting sensors that were considered for use in the study:

Ultrasonic Sensors use the time interval between sending and receiving an ultrasonic wave to detect distance. Typically, these sensors are used for long rage application and are not recommended for use with distances less than 150 mm,

according to data sheets for multiple kinds. Because they output a cone, it is not advised to use multiple ultrasonic sensors in close proximity to each other because the signals can interfere with each other. They can also misread data for sound-absorbing objects.

Infrared Sensors detect infrared radiation reflected from an object. They are typically used for proximity detection rather than for measuring distance. Readings for these sensors are affected by light and the reflectivity of the surface it is reading from.

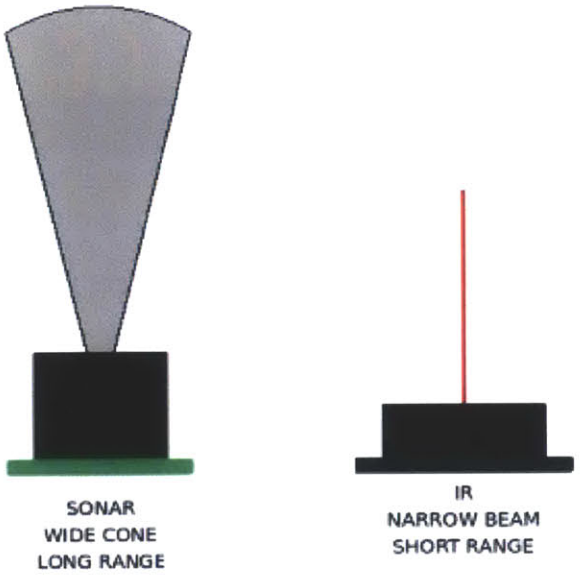

Figure 4.9: Difference in signal emitted by an ultrasonic and infrared sensor. Photo taken from [17].

Sharp Infrared Sensors send out an LED pulse and measure distance based on a triangulation method shown in Figure 4.9.

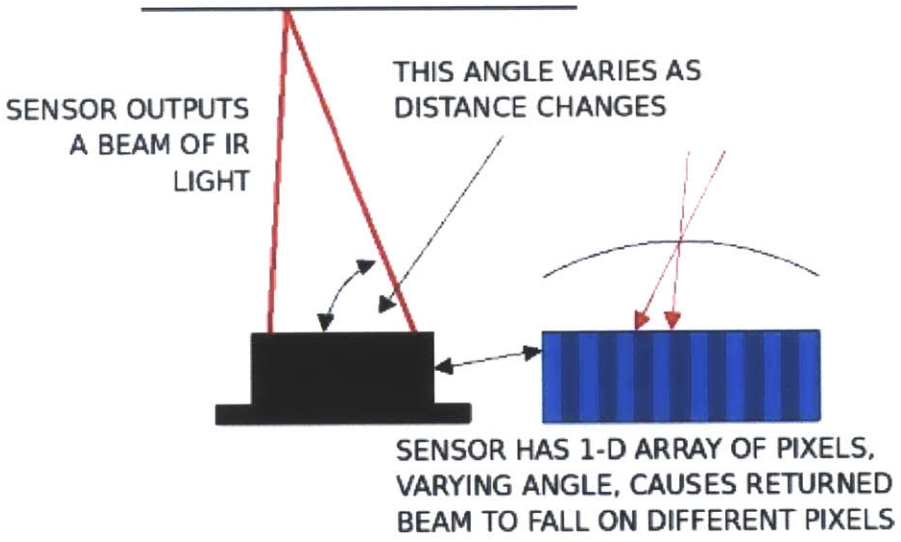

Figure 4.10: Triangulation method that detects distance for Sharp Infrared sensors. Image taken from [17].

4.3 Infrared Sensor Selection

Sharp infrared sensors were chosen for this study for their ability to measure distance and because they could be used in close proximity to each other without interfering with each others signal readings.

The following two infrared sensors were considered for use in this study: the VCNL4000 Infrared Proximity Breakout Board and the SHARP Proximity Short Range Sensor. Both sensors are pictured in Figure 4.10. The VCNL4000 a distance detecting range for distance between 40 to 300 mm and has an I2C interface [14]. The SHARP proximity sensor has a distance detecting range of up to 200 mm [15]. Neither sensor explicitly stated what their specifications for spatial resolution was on their data sheets. The sensors were therefore selected based on their distance detecting range. Both sensors had the smallest distance detecting range compared to other infrared sensors on the market found by the author. Although the distance detecting range was used to select sensors for the study, a better selection method would be the spatial resolution of the sensor. The distance sensing metric is more commonly used to determine at what approximate distance can the robot detect whether or not an object is in its line of vision. Further recommendations for the selection of a well-suited distance measuring sensor for this robot are explained in Chapter 6.

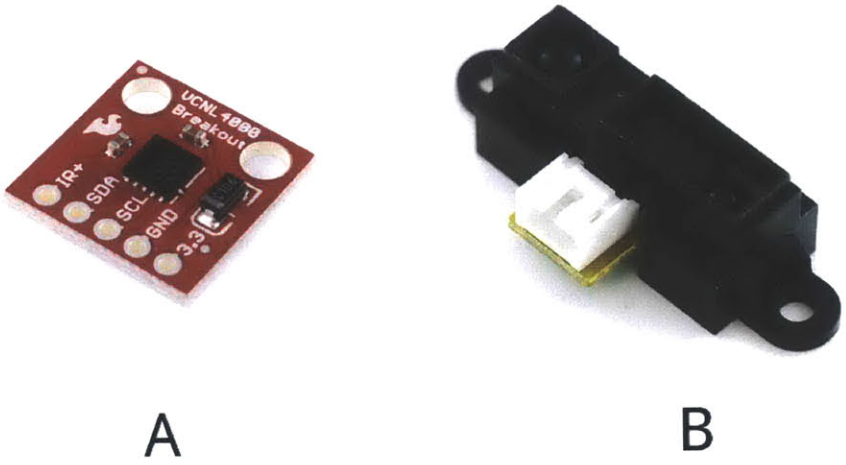

Figure 4.11: Figure on the left is the VCNL4000 Infrared Proximity Breakout Board manufactured from Vishay and sold from Sparkfun. Image on the right is of the SHARP GP2Y0A41SK0F infrared proximity sensor distributed by Sparkfun. Images taken from [18].

Chapter 5

Testing and Analysis

The positional accuracy of the end-effector of the robot is very important. The robot must be able to detect how far away it is from a surface, move to a desired position, and maintain a specified distance D from the surface it is measuring.

To better understand the capabilities of the selected infrared sensors for such functionality, the sensors were calibrated and tested to find a relationship between the output readings of the sensors and the distance between the surface being measured and the sensor.

5.1 Calibration

Both infrared sensors were calibrated to determine the relationship between the distance and the sensor output. To calibrate, each sensor was fixed in place while a flat surface was brought closer to or further away from it with a micrometer stage. The maximum distance between the sensor and the surface was limited by the 26 mm travel distance provided by the micrometer stage. The calibration plots for the

VCNL4000 IR sensor and the SHARP Proximity Sensor can be found in Figures 5.1 and 5.2 respectively. It should be noted that each sensor gave a range of readings at each point at which a measurement was taken. The values plotted in the following graphs represent the average sensor value for each distance measured.

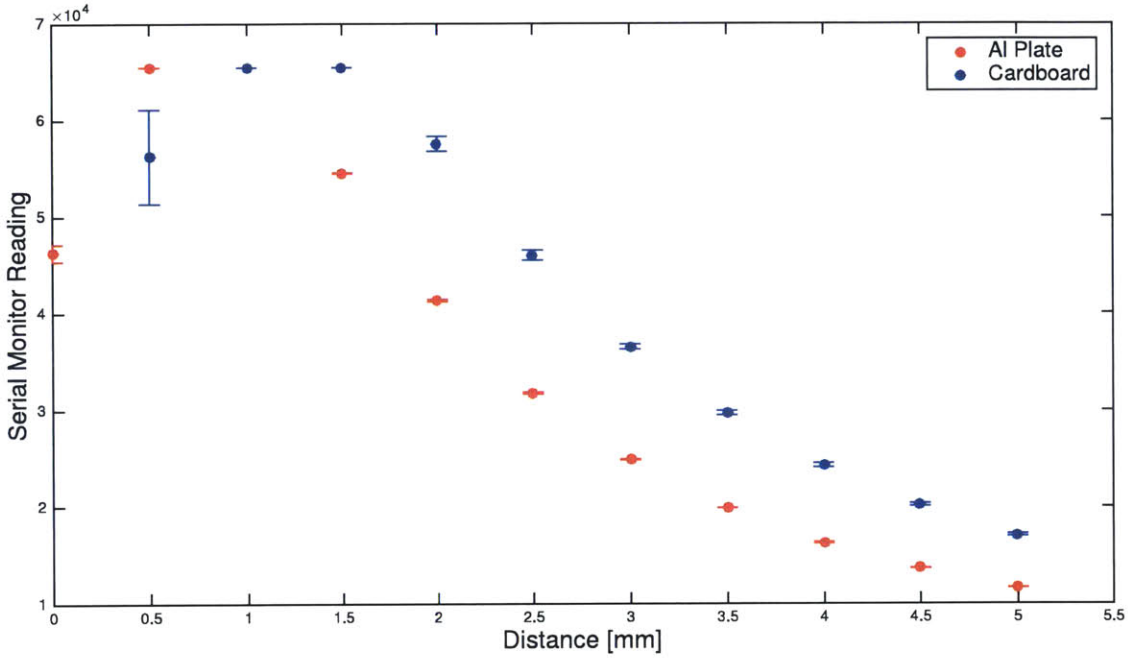

Figure 5.1: Calibration plot for the VCNL4000 IR sensor. The VCNL4000 sensor was calibrated with two different surfaces, an aluminum plate and a piece of brown cardboard. This was done to see how the readings differ for surfaces with difference in reflectiveness because IR sensors are sensitive to ambient light and reflective surfaces. The test was run 5 times. The mean sensor value is represented by a dot on the plot and the standard deviation is represented by the error bars.

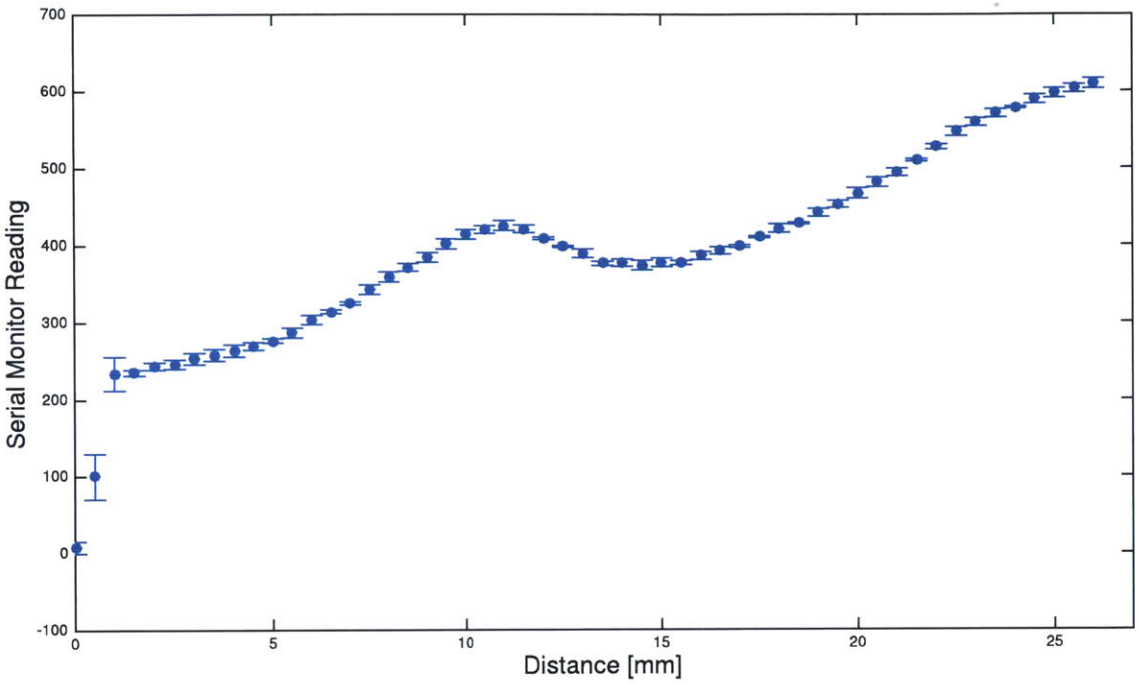

Figure 5.2: Calibration plot for the SHARP Proximity Sensor made with a white cardboard surface. A linear fit was applied to the plot. It was decided to calibrate against a white surface to find representative data of the correlation between position and sensor readings. Calibration should be done again in future work with a surface with similar reflectivity as the skin.

Calibration data for the VCNL4000 were collected over a distance of 0 mm to 5 mm away from the sensor. Only a small range of data was collected because the test was preliminary and only meant to determine connection with the Arduino Uno. It was discovered shortly after that due to the I2C interface the sensor used and the address it was assigned to in the Arduino, only one sensor could be connected to the Arduino at a time. Given that the design requires the use of at least three sensors, it was decided not to pursue the use of the VCNL4000 sensor.

As shown in Figure 5.2, the SHARP proximity sensor was calibrated along the entire length provided by the micrometer stage, a distance of 26 mm, with a piece of white cardboard. The sensor was only calibrated with one surface because infrared sensors are sensitive to ambient light and the reflectivity of the surface it is measuring from. Future work will require the calibration be done with a surface that is has similar reflective properties as the skin.

5.2 Distance Measurements at Fixed Position

Aside from the resolution and range of the distance sensing capabilities of the sensor, it is also important to characterize the accuracy of the sensor readings because that is what determines the measured distance to a surface.

Although the calibration curves found in the previous section show a relationship between the sensor readings from the serial port of the Arduino and the distance to a surface, it was noticed that the sensor gave a range of readings for a given position. To explore the range of values and what distance they correspond to, a test was performed to characterize the variability in readings for a fixed and known position.

For this experiment, a white sheet of paper similar to the one used for calibration was placed underneath the line of vision of the sensor, shown in Figure 5.3. The sensor was in a fixed position while the sensor took measurements for 5 seconds at a sampling rate of 1 kHz.

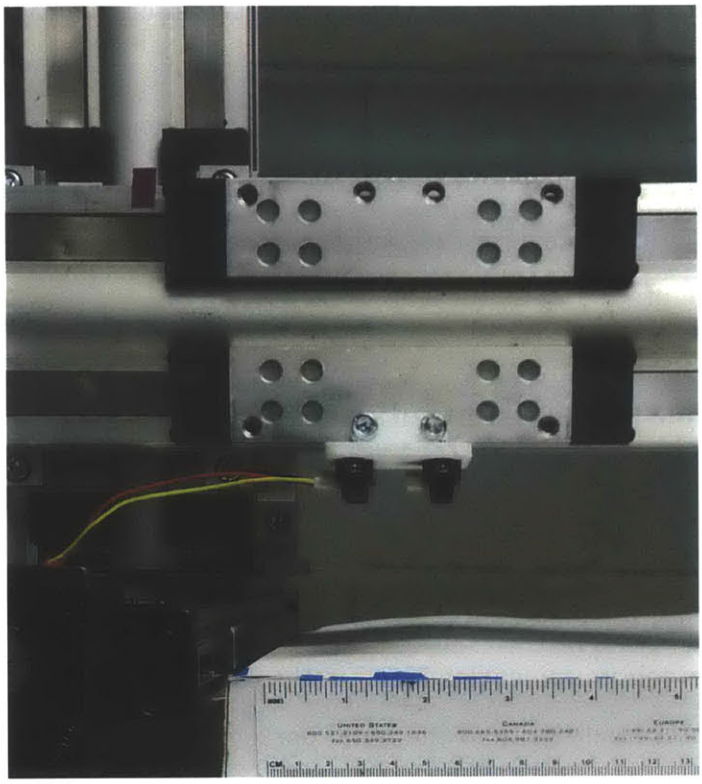

Figure 5.3: Experimental Setup for fixed sensor measurements.The sensors are 52.25 mm from the surface of the white paper.

The distance from the sensor to the surface was measured with ImageJ software to be 52.25 mm. The sensor readings from the Serial Port of the Arduino at this location ranged from 632 to 692 with an average reading of 644 and standard deviation of 8. A linear fit was made to the plot in Figure 5.2 to convert those values to distance measurements. A linear fit was selected because compared to the distance detecting range of the SHARP sensor, the calibration was done over a small distance. Figure 5.4 shows the linear curve fit to the SHARP sensor calibration data.

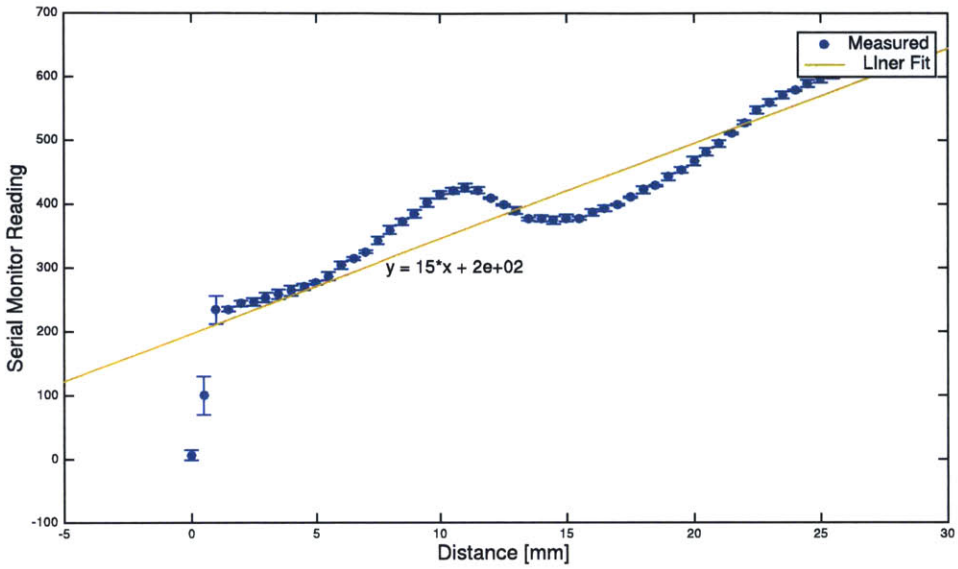

Figure 5.4: Plot of the calibration data for the SHARP Proximity sensor with a linear curve fit to the data.

5.2.1 End-Effector Z Position Placement

Because the sensor readings vary within a range for a set distance from a surface, it is expected that if the end-effector was told to move to a specific Z position, the location would not be precise. This is because the specified position to move to depends on the sensor readings, which can vary for a given position by 60.

The fitted calibration curve converted the sensor readings to correspond to a range of distance measurements from 28.8 mm to 32.8 mm with an average reading of 29.6 mm. These values show that the fitted calibration curve does not provide a good relationship between sensor readings and the distance the sensor is from the measured surface because the actual distance from the sensor to the white paper is 52.25 mm. To explore the range and variability of the sensor readings for a given

position, the sensor must be calibrated for the entire length of the Z-axis and a different curve must be fit to the data.

Chapter 6

Conclusions and Future Development

A 4-degree of freedom robot was designed to position and orient its end-effector to stay parallel to a surface. It was specifically designed for use with a double nozzle hydro-surgical debridement tool to remove necrotic tissue along a wound. However, this study focused on testing the positional capabilities of the end-effector without the rotational degree of freedom.

Two infrared sensors were used to measure the distance between themselves and the surface they are measuring distance from. Neither the VCNL4000 nor the Sharp Proximity Sensor were found to be well-suited to accurately measure the distance between the end-effector and the surface it was measuring from. Both sensors had significant variability in their readings that made it difficult to measure the position it was at. A linear fit was made to the SHARP proximity sensor to provide a relationship between sensor readings and position, but it provided differences in the measured position versus the actual position of about 22 mm. Successful sensor

calibration is needed for future tests to characterize the positional accuracy of the robot. Such calibrations should be done with the sensor mounted on the robot design and measurements should be taken along the entire length of the Z-axis. Calibrating along the length of the Z-axis will help determine whether more than one calibration curve is needed- one that describes the relationship between position and sensor readings within the distance detection range of the sensor and one for positions outside of the range.

6.1 Testing Repeatability and Accuracy of End-Effector Positioning

With a satisfactory calibration curve for the sensor, experiments should be done to characterize the repeatability and accuracy of the of the end-effector to position itself to a given location. The following experiment was designed by the author to test the repeatability and accuracy of the end-effector on a flat surface with a rigid and non-rotating sensor plate.

The robot's end-effector should be placed at a desired and easily accessible position which will be referred as the start position. The distance between the surface and the sensor, as well as the sensor readings for that location will be recorded and the location marked. Then, because the robot is designed to move down towards a surface, the end-effector will be offset 100 mm above the start position. Once the end-effector has moved up along the Z-axis, it will be instructed to move to the start position based purely on the sensor readings. The position at which it stops at and the sensor readings at that position will be measured and compared to the desired position and corresponding expected sensor readings. The experiment should be

done a number of times and should also be done for different offset distances from the start position.

6.2 Alternative Distance Measuring Sensor

The reflectivity of a surface can affect the readings of an infrared sensor. Therefore, skin reflectivity should be taken into consideration for calibration of the sensor if an infrared sensor will be used in future iterations of the robot.

However, it is recommended to consider a different type of sensor for use with hydro-surgical debridement robot. This study focused on the selection of a non-contact sensor to measure distance. If that type of sensor is still desired for the project, then investigation of a laser sensor is recommended, due to its high resolution. The sensor would have to be tested for its distance measuring capabilities. Contact sensors should also be considered for the robot. For example, a force sensor could be used to find a correlation between the force nozzles exert on the wound to the distance they are away from the surface of the wound.

The resolution, sensing range, and the interface with the micro-controller should be considered when selecting a new sensor such that it has less than 1 mm of resolution and a sensing range appropriate for the body part it will be used for. The micro-controller used with the sensor should be compatible with the current and voltage ratings of the sensor and its resolution.

6.3 Additional Degrees of Freedom and Tissue Detection

Future design iterations of the robot should include additional degrees of freedom, as specified in Chapters 3 and 4. Once a suitable sensor is selected for use with the robot, the rotational degree of freedom explained in Section 4.1 should be incorporated into the design of the robot. Testing should then be done to characterize how well the sensor plate is oriented relative to the surface being traced. Once additional degrees of freedom are incorporated into the design, non-flat surfaces can be introduced for use during testing.

Lastly, to develop this positioning robot into a debridement robot, the tissue removal device must be integrated into the design such that testing can be done to determine how well the robot can remove dead tissue from a wound.

Bibliography

[1] Schultz, G., Sibbald, R., Falanga, V., Ayello, E., Dowsett, C., Harding, K., Romanelli, M., Stacey, M., Teot, L., and Vanscheidt, W., "Wound bed preparation: a systematic approach to wound management," Wound Repair and Regeneration, vol. 11, no. 2, 2003.

[2] McFarland A, Smith F., "Wound Debridement: a clinical update," Nursing Standard, vol. 28, no. 52, pp. 51-58, 2014.

[3] Falanga, V, Brem, H., Ennis, W., "Maintenance debridement in the treatment of difficult-to-heal chronic wounds," Ostomy/Wound Management, vol. Supplement 2, no. 13, 2008

[4] Nusbaum A, Gil J, Rippy M, et al. "Effective Method to Remove Wound Bacteria: Comparison of Various Debridement Modalities in an In Vivo Porcine Model," Journal of Surgical Research, vol. 176, no. 2, pp. 701-707, 2012.

[5] Kehoe, B., Kahn, G., Mahler, J., Kim, J., Lee, A., Lee, K., Nakagawa, K., Patil, S., Boyd, W., Abbeel, P., and Godlberg, K., "Autonomous Multilateral Debridement with the Raven Surgical Robot," in Proc. IEEE Int. Conf. Robotics and Automation (ICRA), 2014.

[6] Mayo Clinic, Basic skin layers.
http://www.mayoclinic.org/basic-skin-layers/img-20006377

[7] Sibbald, RG, Williamson D, Orsted HL, Campbell K, Keast D, Krasner D, Sibbald D. Preparing the wound bed- debridement, bacterial balance and moisture balance. Ostomy/Wound Management, vol. 46, no. 11, pp. 14-22, 2000.

[8] Brown, A.A. "A device for debridement using high pressure water jets." MS thesis of Massachussetts Institute of Technology, Cambridge, 2014. DSpace@MIT. Web. 17 Apr. 2015

[9] Printed Dreams, —Kit A03— - BCN3DR.
http://printeddreams.es/wp-content/uploads/2014/11/BCN3D-2-printeddreams.jpg

[10] Pugh method or decision-matrix method.
http://www.enge.vt.edu/

[11] Dassault Systems. Solidworks.
https://www.solidworks.com/

[12] 400XR Series Precision Linear Positioners. Parker Hannifin Corporation, Electromechanical Division, Rohnert Park, CA.
http://divapps.parker.com/divapps/emn/pdf/XR/XRCatalog2.pdf

[13] Zeta Drive Installation Guide. Parker Hannifin Corporation, Electromechanical Division, Rohnert Park, CA.
http://divapps.parker.com/divapps/

[14] VCNL4000. Vishay Semiconductors, Malvern, PA.
http://cdn.sparkfun.com/datasheets/BreakoutBoards/vcnl4000

[15] SHARP GP2Y0A41SK0F Datasheet. SHARP Electronics Corporation, Osaka, Japan.
http://cdn.sparkfun.com/datasheets/Sensors/Infrared/GP2Y0A41SK0F

[16] Ardiuno, Ardiuno Uno.
http://www.arduino.cc/en/Main/ArduinoBoardUno

[17] Trossen Robotics, Tutorial: Choosing Sensors for Your Robot.
http://forums.trossenrobotics.com/tutorials/

[18] Sparkfun, Niwot, CO
http://sparkfun.com/